

KfK 3344
April 1982

Laser Induced Fluorescence Spectroscopy in Atomic Beams of Radioactive Nuclides

H. Rebel, G. Schatz
Institut für Angewandte Kernphysik

Kernforschungszentrum Karlsruhe

KERNFORSCHUNGSZENTRUM KARLSRUHE

Institut für Angewandte Kernphysik

KfK 3344

LASER INDUCED FLUORESCENCE SPECTROSCOPY IN
ATOMIC BEAMS OF RADIOACTIVE NUCLIDES

H. Rebel and G. Schatz

Kernforschungszentrum Karlsruhe GmbH, Karlsruhe

Invited Talk presented at the Conference on
Lasers in Nuclear Physics, April 21-23, 1982
Oak Ridge, Tennessee

Als Manuskript vervielfältigt
Für diesen Bericht behalten wir uns alle Rechte vor.

Kernforschungszentrum Karlsruhe GmbH
ISSN 0303-4003

ABSTRACT

Measurements of the resonant scattering of light from CW tunable dye lasers, by a well collimated atomic beam, enable hyperfine splittings and optical isotope shifts to be determined with high precision and high sensitivity. Recent off-line atomic beam experiments with minute samples, comprising measurements with stable and unstable Ba, Ca and Pb isotopes are reviewed. The experimental methods and the analysis of the data are discussed. Information on the variation of the rms charge radii and on electromagnetic moments of nuclei in long isotopic chains is presented.

Laser-Fluoreszenz-Spektroskopie an Atomstrahlen radioaktiver Nuklide

ZUSAMMENFASSUNG

Messungen der Resonanzfluoreszenzanregung an kollimierten Atomstrahlen mit Hilfe von durchstimmbaren Farbstofflasern ermöglichen die Bestimmung von Hyperfeinstrukturaufspaltungen und Isotopieverschiebungen optischer Spektrallinien mit hoher Genauigkeit und Empfindlichkeit. Neuere Atomstrahl-Experimente mit äußerst geringen Substanzmengen der Meßproben, Messungen an stabilen und radioaktiven Ba-, Ca- und Pb-Isotopen werden geschildert. Die experimentellen Methoden und die Analyse der Daten werden beschrieben, und die Information über die Variation der mittleren quadratischen Ladungsradien der Atomkerne und ihre elektromagnetischen Momente wird diskutiert.

I. INTRODUCTION

The main difficulty met in hyperfine spectroscopy of artificially produced radioactive nuclides is that these nuclides are available only in a limited supply for a limited time. The application of extraordinary light sources such as highly monochromatic, tunable lasers is certainly of considerable significance to overcome the limitations of classical optical spectroscopy. However, there is no generally valid, unambiguous answer to the question which special spectroscopic technique has to be preferred for a particular case, hence requiring a careful analysis of the overall sensitivity of the experimental method under consideration. The variety of efficient laser spectroscopic methods presented at this meeting reflects not only the fascination of lasers and their appeal to our imagination, but also the large variety of experimental situations.

Experiments with radioactive nuclides make often use of the fact that the nuclides can be provided as a collimated beam avoiding window-problems and wall-adsorption in sealed-off cells. This enables also a natural laserspectroscopic adaptation of the atomic-beam light source ¹ designed to minimize the Doppler broadening due to thermal motion of the atoms, by exciting or observing resonance fluorescence in a direction perpendicular to the beam. In most laserspectroscopic methods one observes the response of the atoms to the tunable monochromatic excitation provided by the laser instead of analyzing the complex light emitted or absorbed by the atoms. Since the excitation can be really considered to be monochromatic, the resolving power of laserspectroscopy is limited only by homogeneous or inhomogeneous line broadening due to the atoms themselves or their environment. In an atomic beam some of these causes of broadening can be greatly reduced, and this is one of the main reasons for using it. The response of the atoms to laser light illumination can be detected by measuring the reemitted fluorescence light by a sensitive light detector. The average transit time of a thermal velocity atom passing transversely through the laser beam is about 10^{-5} - 10^{-6} s whereas

the lifetime of an excited resonance level is typically in the order of 10^{-8} s. Hence a single atom can be excited repeatedly, and due to the high interaction cross sections of the order of 100 Mbarns and due to the spectral brightness of the laser source, it is easy to get 100 resonance photons from each atom during its transit. This feature establishes the enhanced sensitivity of laser induced atomic beam fluorescence spectroscopy. Greenlees et al.² have developed a method increasing the overall efficiency of fluorescence detection by exploiting the time correlation of the photon bursts.

The present talk considers some representative examples of isotope shift and hyperfine structure measurements by atomic beam laserspectroscopy of stable and radioactive nuclei in isotopic chains of barium^{3,4} calcium⁵ and lead^{6,7}. The experiments were performed at the Karlsruhe Isochronous Cyclotron, but are not coupled "on-line" to the accelerator and up to now restricted to half-lives of some minutes. The studies aim at size and shape information on nuclear charge distributions and are in context of gamma-spectroscopic investigations of transitional nuclei⁸ and alpha-particle scattering studies^{9,10} of nuclear matter distributions in Ca and Pb.

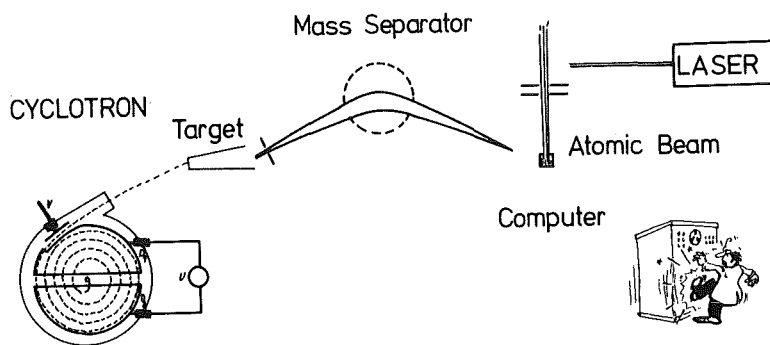


Fig. 1 Atomic beam laser spectroscopy in the neighbourhood of an accelerator.

The unstable nuclides were produced via compound nuclear reactions by charged particle irradiation of appropriate targets or by activation in the flux of thermal neutrons of a reactor (Karlsruhe FR2). The access to the radioactive Ca isotopes is neutron or charged particle activation of stable neighbours of the same element which enhances the impurity problems of the samples. ^{210}Pb was available from the decay of the radioactive ^{238}U family. The production processes are not very isotope selective so that a subsequent enrichment by an electromagnetic mass separator has been necessary (Fig. 1). The necessity of an efficient mass separation is obvious when considering an estimated fluo-

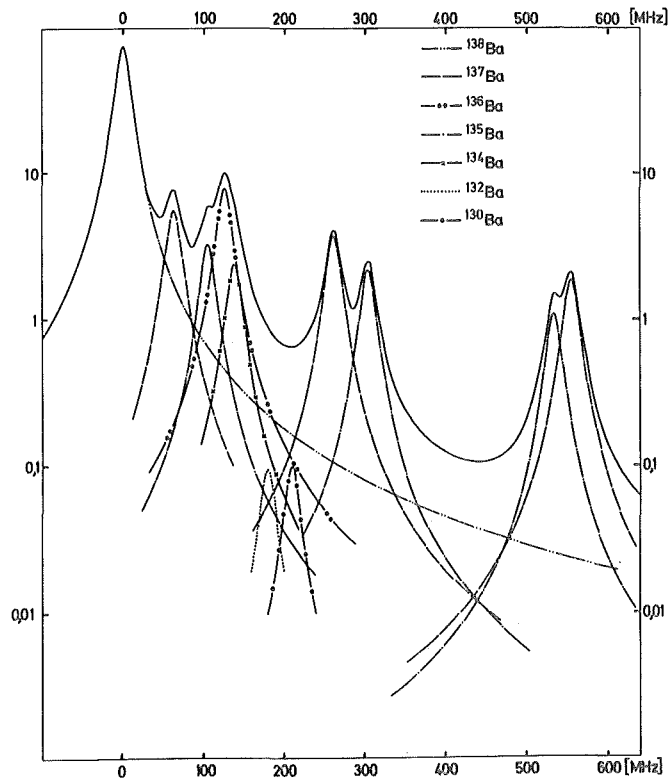


FIGURE 2. Theoretical fluorescence spectrum of a natural mixture of stable Ba isotopes.

rescence spectrum of a natural mixture of stable Ba isotopes (Fig. 2), calculated with the natural line width of 19 MHz. Due to small shifts and the long tails of the Lorentzian line shapes an unambiguous assignment requires the isolation of the interesting isotope. This is even true for heavy elements since the presence of large amounts of stable isotopes would obscure the hyperfine splitting of less abundant radioactive nuclides.

After mass separation samples of 10 pg to a few ng were ready for producing the atomic beams. In order to value such small quantities, we may realize, that the average concentration ¹¹ in normal air amounts to ca. 20 ng/m³ Ba, 0.7 µg/m³ Pb and 0.9 µg/m³ Ca.

II. FLUORESCENCE SPECTROSCOPY OF NEUTRON DEFICIENT BA NUCLEI

In addition to the alkalines, especially sodium, the isotopes of barium seem to be favoured by optical spectroscopists, even if particularly small isotope shifts have rendered precise determinations more difficult (see ref. 12 and references given there). The experimental set-up used in Karlsruhe ^{3,4} for investigations of the BaI ($6s^2 \ ^1S_0 \rightarrow 6s6p \ ^1P_1$, $\lambda = 553.6 \text{ nm}$) resonance transition is schematically shown in Fig. 3.

It consists of an apparatus producing a highly collimated beam of radioactive atoms and a second reference beam operated with a stable isotope. The atomic resonance transitions of the green Ba line are induced by two tunable high resolution CW dye lasers in single mode operation. One dye laser is locked to the transition frequency

of the stable isotope in the reference atomic beam and provides an optical reference frequency. The frequency of the other laser is tuned through the resonance and excites flu-

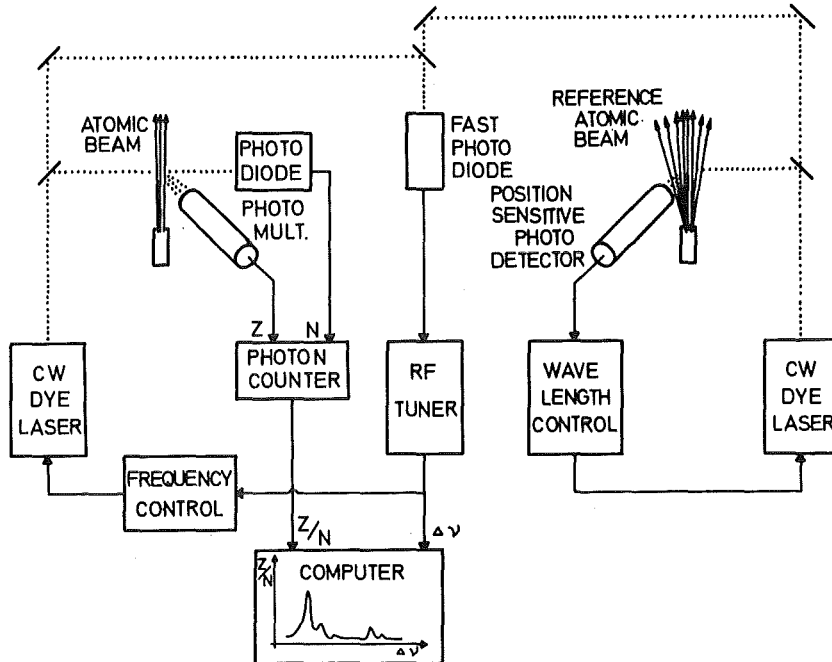


FIGURE 3. Schematic view of the experimental set-up, used for atomic beam fluorescence spectroscopy of Ba nuclides

orescence of the radioactive atoms. It is controlled by stabilizing the difference of the two laser frequencies. This is achieved by mixing the light of the two laser beams on a fast photodiode, the photo current of which is then modulated with the difference frequency. The difference frequency is compared with the output signal of a calibrated r.f. generator. This heterodyne technique enables most precise measurements of optical frequencies.

The fluorescence intensity is measured by a single photon counter. Monitoring, data acquisition and control of the experiment are done by a computer interfaced to the experiment. Fig. 4 displays a typical fluorescence spectrum measured for the $I=11/2^-$ isomer and the groundstate of ^{133}Ba in presence of some impurities of stable barium. The line width (separately measured with a pure sample) of 21.5 MHz is only 10 % larger than the natural line width and justifies a least square fit analysis with pure Lorentzian shapes. However, power broadening and optical pumping effects have to be avoided. On the other side optical pum-

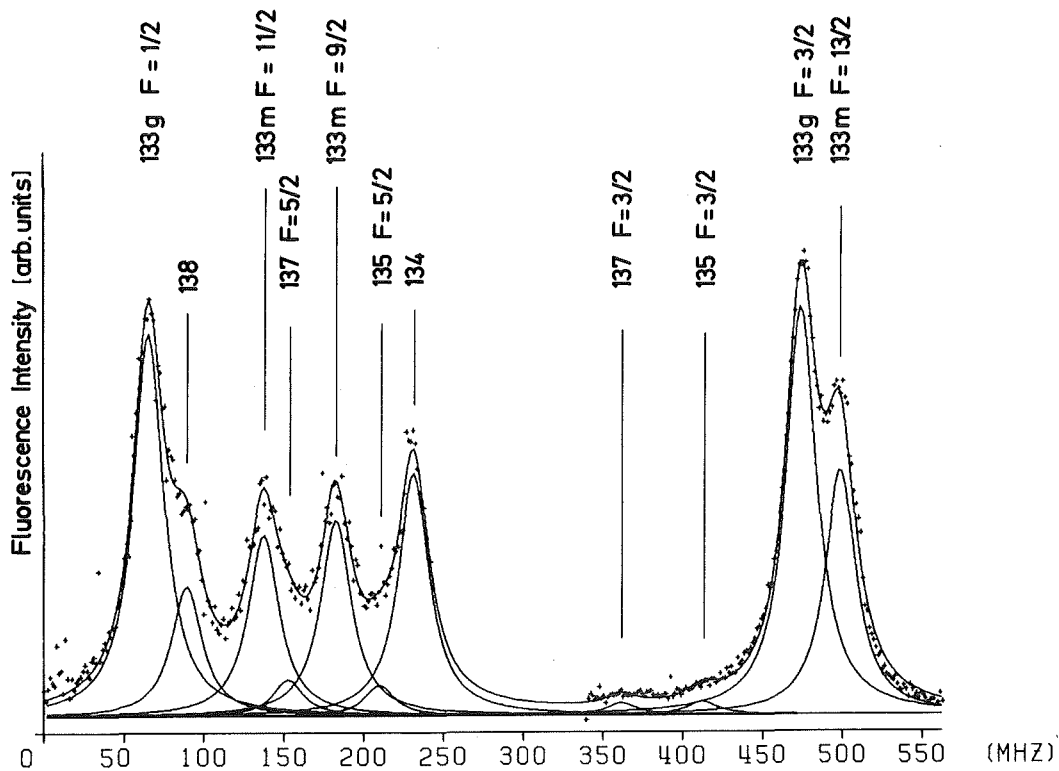


FIGURE 4. Fluorescence spectrum of a $^{133}\text{g+m}$ sample.

ping provides a useful method for identifying and assigning the different hyperfine (hfs) components. Exciting the three 1P_1 hfs component ($F=I, I+1$) by linearly polarized laser light, only $\Delta m_F=0$ transitions are allowed thus saturating the lowest ($F=I-1$) component. In Fig. 5 it is shown that one component relatively decreases when the intensity of the laser π -light is increased. Please note in Fig. 4 the strong violation of Lande's interval rule, just changing the sequence of the hfs components and directly revealing a large spectroscopic quadrupole moment of the isomeric state.

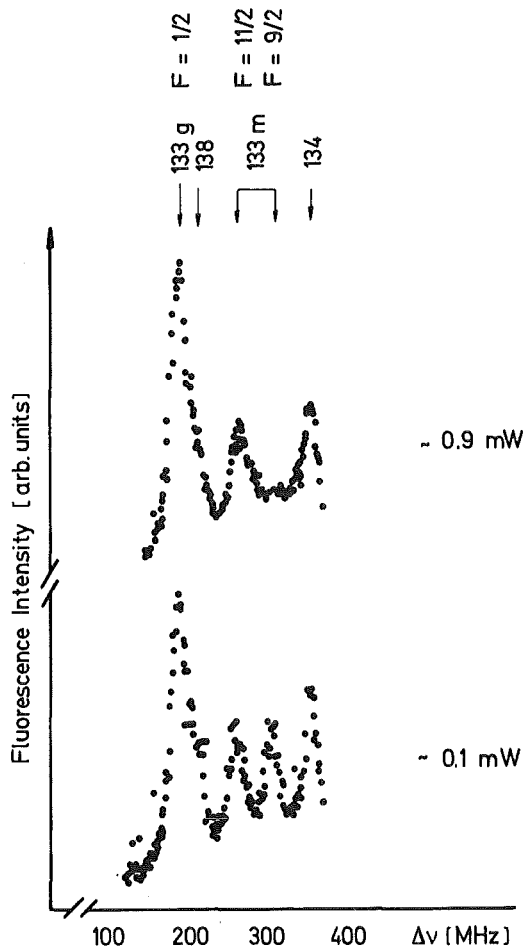


FIGURE 5.
Parts of two fluorescence spectra showing optical pumping of the $F=9/2$ hfs component in $^{133m}\text{Ba}(I=11/2)$ when irradiated with linearly polarized laser light.

A similar result is present in the case of ^{135m}Ba . The measurement of ^{124}Ba ($T_{1/2}=11.9$ m) is an example of the extreme sensitivity achievable by the method. This particular case, where all fluorescence spectra were taken with a 10 pg sample, an analysis in view of the probable experimental limits of sensitivity has been performed¹³. It seems not too optimistic to say that measurements are rather well feasible with 1 pg, at least for even Ba isotopes (where hyperfine splitting is absent).

As well known, when deriving from optical isotope shifts information about nuclear charge distributions, we meet the problem to calibrate the measured shifts (of a particular optical transition i) between the isotopes A and A'

$$\delta v_i^{AA'} = F_i \lambda^{AA'} + \left(\frac{1}{A} - \frac{1}{A'}\right) S_i$$

in terms of charge radii differences $\delta\langle r^2 \rangle$.

The isotope shift is split in the volume effect carrying the nuclear structure information by the nuclear parameter

$$\lambda^{AA'} = \delta\langle r^2 \rangle^{AA'} + \frac{C_2}{C_1} \delta\langle r^4 \rangle^{AA'} + \dots,$$

and the mass shift which includes a nontrivial part from the specific mass effect and is actually subject of various uncertainties¹². It has been pointed out¹⁴ that the ratios of the constants C_n are equal in X-ray and optical transitions. This implies that optical isotope shifts and X-ray shifts in ordinary atoms are sensitive to the same nuclear moments ($\lambda^{AA'} \cong \delta\langle r^2 \rangle^{AA'}$, as higher radial moments contributions are negligible for $Z=56$). Unfortunately, electronic X-ray shifts in stable Ba atoms have not been measured

with sufficient accuracy¹⁵. We have related the isotope shift measured for the $\lambda=553.6$ nm BaI transition to the data known for stable isotopes for the $\lambda=493.4$ nm BaII ($6s\ 2S_{1/2}-6p\ 2P_{1/2}$) transition¹⁶ via a King plot

$$\frac{A \cdot A'}{A' - A} \delta v_I^{AA'} = \frac{F_I}{F_{II}} \frac{A \cdot A'}{A' - A} \delta v_{II}^{AA'} + (S_I - S_{II} \frac{F_I}{F_{II}})$$

The point is that for the BaII line, an alkali-like transition, the electronic factors are expected to be calculated more reliably. The calibration factors for the BaI shifts resulting from the combination are in good agreement with semiempirical systematics. Realistic estimates of the uncertainties are quite difficult. Heilig and Steudel¹⁷ concluded from systematic studies that the specific mass effect in this type of transitions is not larger than the normal shift (nms). Therefore, we scaled our data somewhat arbitrarily by assuming the specific mass shift = 0, but within the uncertainty of ± 1 x nms. This procedure proves to be consistent with all further information provided by atomic structure calculations and the systematic behaviour of nuclear charge radii¹⁸. However, we are embarrassed when introducing muonic X-ray shifts, recently measured with high accuracy for ^{138,136,134}Ba and reported¹⁹ as preliminary results. If using the nuclear parameters ($\delta\langle r^2 \rangle$) deduced in a slightly model-dependent way from the Barrett moments, unbelievable electronic factors and an unreasonably rapid variation of the charge radii would come to light, and the resulting difficulties would appear to be a problem of interpreting muonic shifts rather than of the uncertainties of the atomic ingredients in optical shifts. Ignoring this problem, Fig. 6 displays the variation $\delta\langle r^2 \rangle$ of the charge radii as extracted from the measurements. The systematic uncertainty due to the specific mass effect obviously dominates the total uncer-

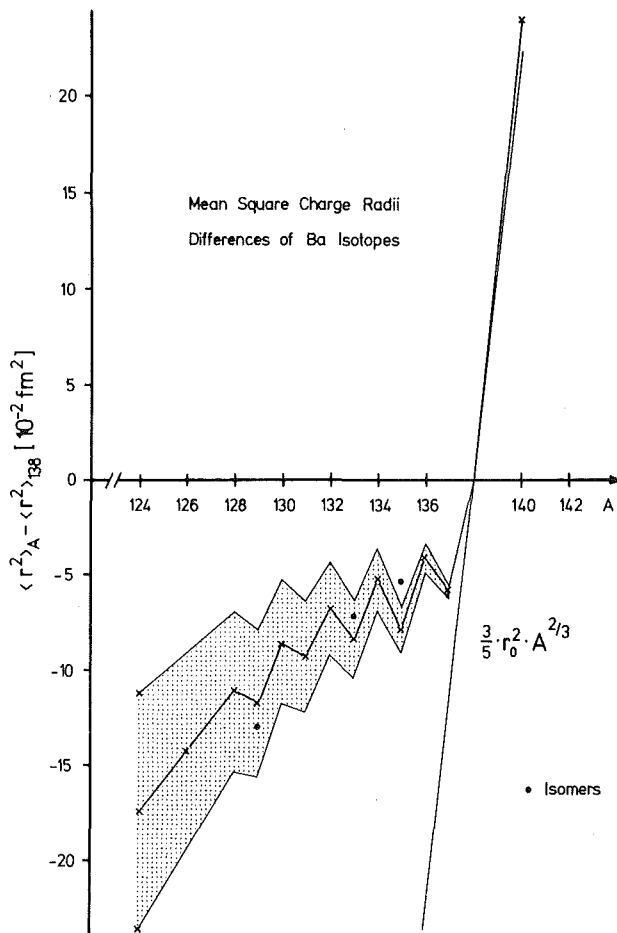


FIGURE 6.
Differences
of ms charge
radii of Ba
nuclei.
The dashed region
indicate the
systematic un-
certainty of
the contribu-
tion from spe-
cific mass ef-
fect. The
value for
¹⁴⁰Ba is cal-
culated from
results given
in ref. 16.

tainty, but does not affect the values for isomeric shifts in ^{135,133,129}Ba. A prominent odd-even staggering is present, and with decreasing neutron number the nuclei shrink by far more slowly than estimated by the $A^{1/3}$ law of an incompressible spherical nucleus. One reason for this feature is an increasing ms deformation on the neutron deficient side. But when controlling the $\langle \beta^2 \rangle$ values by measured B(E2) values we have additionally to require variation of the monopole part of $\delta \langle r^2 \rangle$. This reflects the "radius anomaly" which is by no means anomalous. The droplet model²⁰ which relates nuclear radii to other gross properties of nuclei

is able to explain the required variation of the monopole term in $\delta\langle r^2 \rangle$ (see ref. 3). A further conspicuous feature is the sudden increase of the ms charge radii after crossing the closed shell. The trend on the neutron rich side is confirmed and continued by recent results from collinear beam spectroscopy²¹, extending the data up to A=146.

In addition to isotopic and isomeric shifts in radii, the studies provide rich information about electromagnetic moments of the odd nuclei. This is discussed in detail elsewhere⁴, but let us emphasize that just a combined consideration of changes in radii and quadrupole moments is able to reveal interesting nuclear structure effects of transitional nuclei²².

III. OPTICAL ISOTOPE SHIFTS OF CALCIUM ISOTOPES

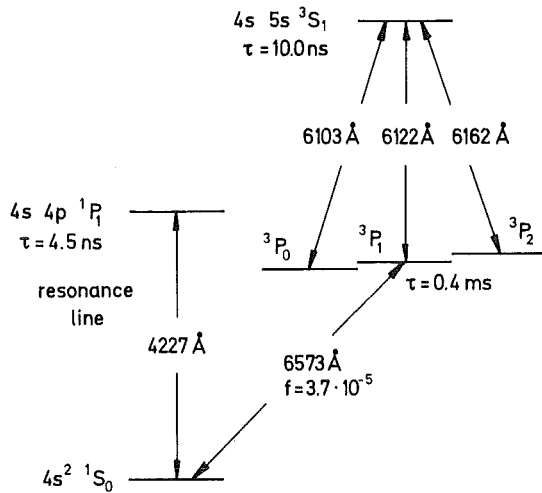
The long isotopic chain between the two doubly magic nuclei ^{40}Ca and ^{48}Ca where the neutron number changes by as much as 40 % provides a unique playground for observing interesting nuclear structure effects associated with the addition of neutrons in the $f_{7/2}$ shell. The charge distribution of stable nuclei has been extensively investigated by electron scattering²³, by muonic X-ray shifts²⁴ and conventional optical isotope shift measurements (see ref. 22 for a compilation). In recent time, there are also serious attempts in determining mass and neutron distributions by means of high energy protons, alpha particles and pions (see ref. 9). The only experimental techniques which are able to extend our knowledge to unstable Ca nuclei are laserspectroscopic methods. In a series of experiments the Heidelberg group²⁵ applied high resolution intracavity

spectroscopy for studying the very weak 657.3 nm ($4s^2\ ^1S_0 \rightarrow 4s4p\ ^3P_1$) intercombination line which has the ad-

FIGURE 7.

Energy level scheme of Ca I

CaI level scheme.



vantage of a rather small natural line width of 410 Hz, but restricting the sensitivity to samples in the range of 10 μg . Using basically the same method and apparatus as with the Ba experiments the Karlsruhe group⁵ studied the blue 422.7 nm ($4s^2\ ^1S_0 \rightarrow 4s4p\ ^1P_1$) resonance transition. Fluorescence spectra were measured with samples of typically 10 ng. The ^{47}Ca sample was smaller (170 pg). In this case, the measuring method was slightly modified in order to avoid optical pumping effects when increasing the laser power. A Pockels cell driven by an rf oscillator was inserted in the laser beam such that the laser light polarization was continuously modulated between parallel and perpendicular to the observation direction.

The measured isotope shifts have been transformed by use of precise values of $\delta\langle r^2 \rangle$ known from electron scat-

tering and muonic X-ray studies²⁴. Due to this calibration the optical values $\delta\langle r^2 \rangle$ are not independent from the muonic data; however, the combination improves also the accuracy of the comparatively imprecise results for ^{43,46}Ca from muonic X-ray data. In addition, by this calibration the specific mass effect proves to be only a 7 % contribution of the Bohr shift.

Fig. 9 compiles different experimental results establishing the peculiar behaviour of the Ca charge radii when filling up the second half of the neutron shell:

- the charge radii of ⁴⁰Ca and ⁴⁸Ca are equal whereas the even nuclei in between have a charge radius larger in size by about 1 %.
- there is a considerable odd-even staggering.
- there is only a minute difference between the charge radii of ⁴⁰Ca and ⁴¹Ca, an interesting fact in view of the discussion of the ⁴¹Sc-⁴¹Ca Coulomb displacement energy, neutron excess radii and core compression effects.

We discuss the nuclear structure information of these results somewhat more in detail in the light of the influence of long-range groundstate correlations (phenomenologically represented by the mean square deformation $\langle \beta^2 \rangle$), of droplet model predictions and simple shell model considerations.

Indeed, there are conspicuously similar trends in the quadrupole transition strength inferred from inelastic alpha particle scattering, in electromagnetic B(E2) values as well as in the transition radii measured for the $0_1^+ - 0_2^+$ monopole transitions by electron scattering (see ref. 22). When

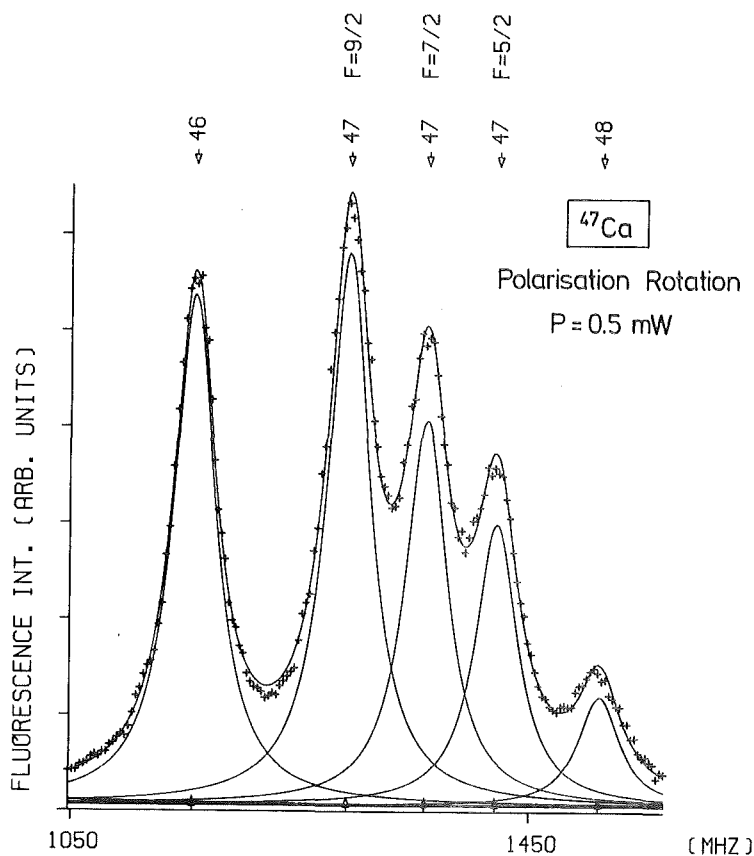


FIGURE 8. Spectrum of a $^{46,47,48}\text{Ca}$ sample containing only $\sim 170 \text{ pg } ^{47}\text{Ca}$ ($T_{1/2} = 4.54 \text{ d}$), introducing into the expression

$$\delta \langle r^2 \rangle = \delta \langle r^2 \rangle_0 + \frac{5}{4\pi} \langle r^2 \rangle_0 \delta \langle \beta_2^2 \rangle$$

the mean square deformation derived from experimental $B(E2; 0^+ \rightarrow 2_1^+)$ values, we find a large part of the variation with the even nuclei attributed to the variation of the quadrupole deformation ($\delta \langle r^2 \rangle_0 \cong 0$). This explanation, however, anticipates the strongest effects to be borne out from

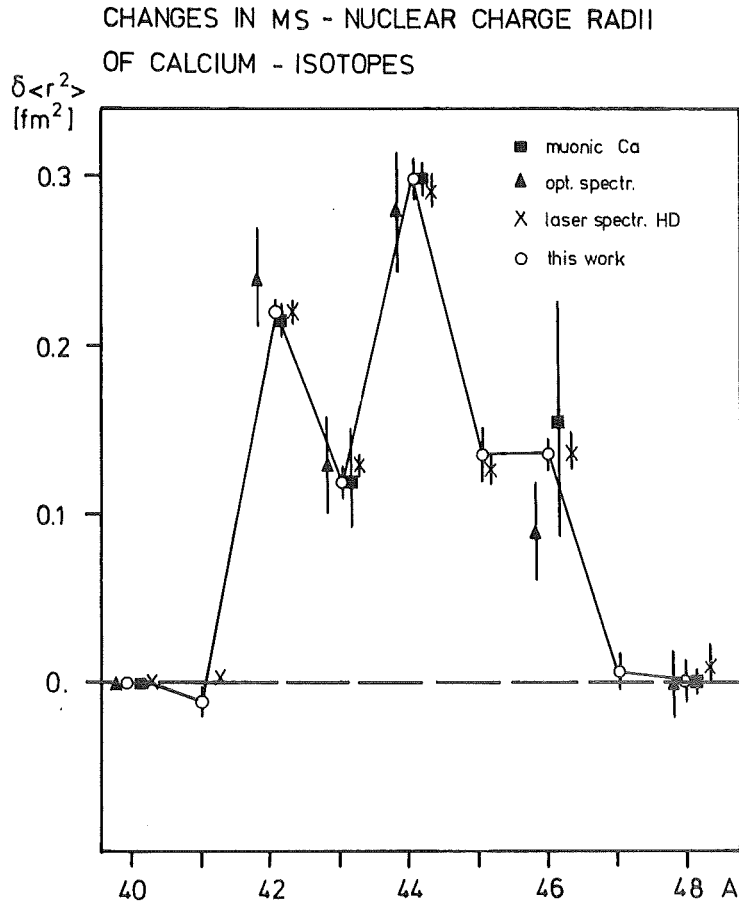


FIGURE 9. Variation of the mean square nuclear charge radii of Ca isotopes.

the $B(E2)$ values of the first 2^+ states neglecting, for example, the marked variation of the octupole strength in Ca isotopes. Another experimental observation, certainly related and revealed by electron scattering²³, is the considerably reduced skin thickness of the charge distribution of ^{48}Ca compared to ^{40}Ca .

We consider these results briefly on the basis of

a convenient parametrization of the nuclear charge distribution, convoluting a homogeneously charge sphere with radius R with a Gaussian of variance σ (Helm's model, see ref. 26)

$$\rho(r) = \int \rho_{h.s.}(\vec{r}', R) \cdot \rho_G(\vec{r}-\vec{r}', \sigma) d^3r$$

In a recent systematic analysis of electron scattering form factors, Friedrich and Voegler²⁷ have demonstrated that the parameter σ is rather accurately related to the skin thickness t of a Fermi distribution $t = 2.54 \sigma$ ($=4.39$ a). Moreover, the extension parameter R proves to be identical with the "diffraction minimum sharp" (dms) radius extracted from the minima of the electron scattering form factor and can be appropriately identified with the proton radius given by the droplet model²⁰. In agreement with experimental dms radii of Ca nuclei (and in contrast to the rms radii) the droplet model radii are increasing monotonically. Consequently the variation the observed variation in the ms radii

$$\delta \langle r^2 \rangle = \frac{3}{5} \delta R^2 + 3 \delta \sigma^2$$

is projected into a "shell effect" of the surface thickness. Fig. 10 displays the variation of the surface diffuseness parameter as required by the experimental $\delta \langle r^2 \rangle$ when combined with the droplet model prediction for δR^2 . We subtract now the contribution from long-range ground state correlations introducing a reduced skin thickness $\tilde{\sigma}$ by

$$\delta \langle r^2 \rangle = \frac{3}{5} \delta R^2 + 3\delta \sigma^2 + \frac{5}{4\pi} \left(\frac{3}{5} R^2 + 3\sigma^2 \right) \delta \langle \beta_L^2 \rangle$$

Deducing $\delta \langle \beta_L^2 \rangle$ from measured quadrupole and octupole transition probabilities (unfortunately not known for all isotopes) following features emerge (Fig. 10)

- the difference in the surface skin thickness of ^{40}Ca and ^{48}Ca can be ascribed to the strong octupole strength in ^{40}Ca
- the difference of the ms radii of ^{40}Ca and ^{48}Ca , corrected by the contributions from ms deformation, is just the value given by the droplet model.

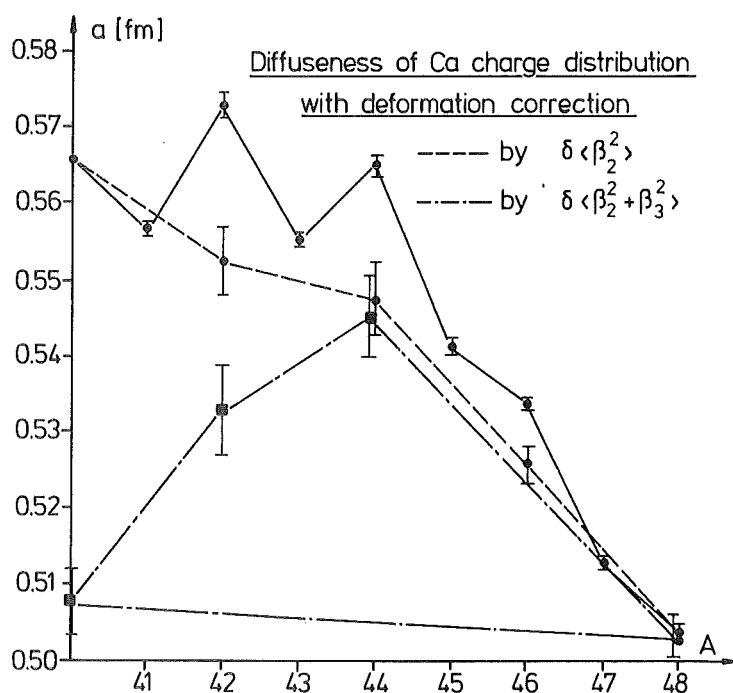


FIGURE 10. Variation of the surface diffuseness of nuclear charge distributions of Ca.

- the correlation between the variation of the ms radii and $B(E2, 0^+ - 2_1^+)$ values appears to be rather fortuitous. The parabolic trend seems to arise from a (unexplained) background remaining in the surface diffuseness.

These features are supported by microscopic approaches of nuclear structure²⁸. In the framework of shell model calculations configuration mixing is going to explain the superimposed odd-even staggering. Talmi²⁹ has proposed a simple model mixing to $(f_{7/2})^n$ shell model states which are based on a $I=0$ core, some other excited states where the $(f_{7/2})^n$

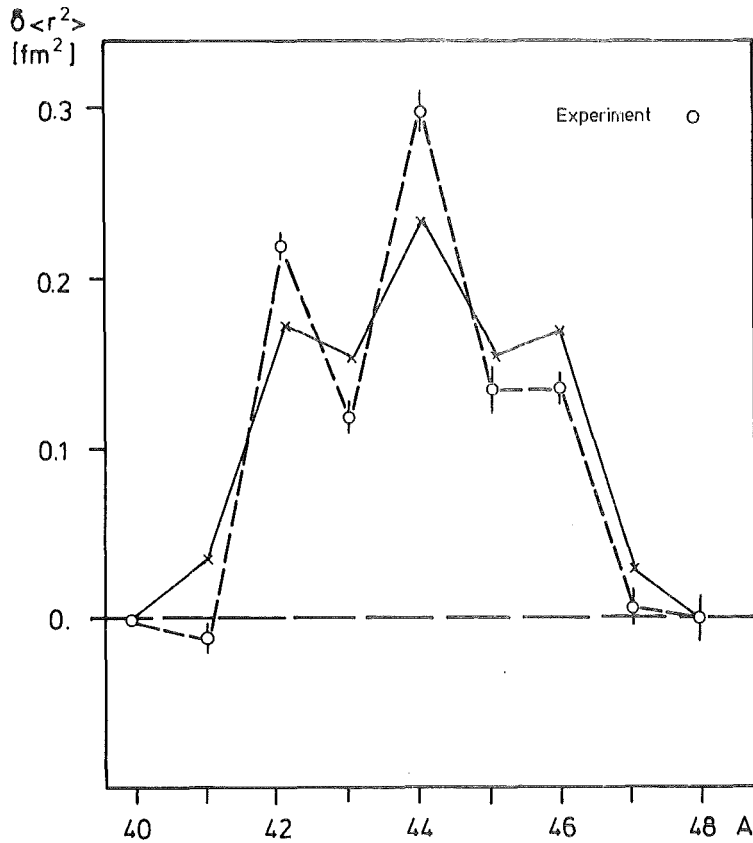


FIGURE 11. Variation of the Ca charge radii seen in Talmi's mixed model.

configurations are coupled to a 2^+ -state (presumably deformed). Assuming that the mixing amplitudes do not depend on further structure effects, the variation $\delta\langle r^2 \rangle$ can be most simply described by two parabolas for even and odd A Ca nuclei.

$$40+n, 40 \delta\langle r^2 \rangle = \begin{matrix} K \cdot n(8-n) & \text{for even A} \\ K \cdot [n(8-n)-4] & \text{for odd A} \end{matrix}$$

It is impressing to see how clearly such an idea reproduces the qualitative features of the experimental observation, thus possibly guiding further theoretical refinements.

IV. HIGH RESOLUTION HYPERFINE SPECTROSCOPY OF STABLE AND RADIOACTIVE LEAD ATOMS

The interest in isotope shifts and hyperfine structure splitting* as source of relevant nuclear structure information on lead nuclides originates from very early spectroscopic studies started by H. Kopfermann³¹ and impressively refined and extended by Brix and coworkers³². Recent experimental work comprises two-photon laser spectroscopy³³ and measurements of electronic K_{α_1} -X-ray shifts of stable isotopes³⁴, highly sensitive atomic beam absorption spectroscopy³⁵ and atomic beam laser spectroscopy^{6,7} applied to short-lived Pb nuclides. In addition, detailed

*Hyperfine structure of Pb lines is known³⁰ since 1909, unexplained at that time when missing any concept of isotopes.

information for the stable isotopes has been obtained by the analysis of electron scattering and muonic X-ray data³⁶.

In our current experiments^{6,7} resonance fluorescence of the $6p^2\ ^3P_0 \rightarrow 6p7s\ ^3P_1$ transition ($\lambda=283.3\text{ nm}$) is excited in a well collimated Pb atomic beam. Coherent tunable CW ultraviolet radiation is generated by frequency doubling the output of a tunable ring dye laser operating in the visible and adjusting the temperature of a nonlinear ADA crystal to maintain phase matching. The conversion efficiency of second harmonic generation, if well 90° -phase matched is of the order of $5 \times 10^{-4}\text{ W}^{-1}$ thus providing typically $200\ \mu\text{W}$

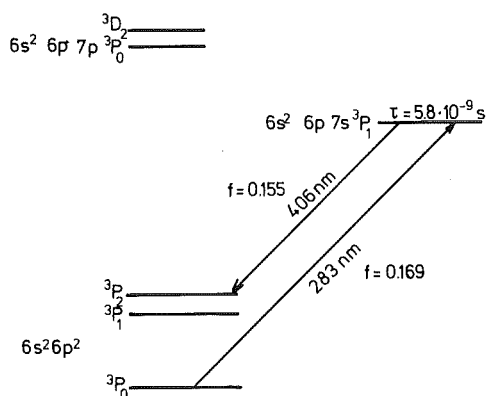


FIGURE 12.
Part of PbI level scheme

with our set-up. The fluorescence is monitored by the decay into the metastable 3P_2 level with $\lambda=405.8\text{ nm}$. This reduces considerably background problems from scattered laser light. On the other side the sensitivity does not profit from multiple excitation of single atoms.

The experimental set-up used for the measurements of the Pb isotopes is schematically shown in Fig. 13. The optical reference frequency provided by the second dye laser is stabilized to a 2 GHz cavity which in turn is stabilized

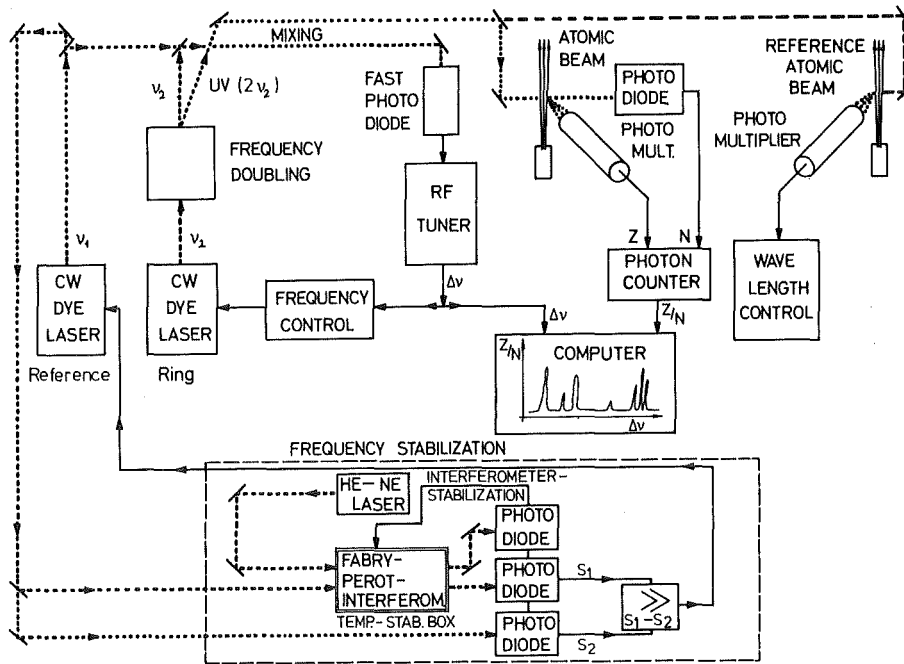


FIGURE 13. Schematic view of the experimental set-up used for spectroscopy of Pb.

to a frequency-stabilized He-Ne-laser. The difference frequency of the dye lasers is again generated by heterodyning with a fast photodiode and a radiofrequency analyzer. The measuring procedure starts with exciting the considered UV transition in a separate reference atomic beam operated with a stable lead isotope and defining the reference frequency with zero difference. Experimental line widths have been obtained of the order of 50 MHz (Fig. 14).

The results up to now obtained comprise^{6,7} isotope shifts and hyperfine structures of 12 stable and unstable Pb isotopes and isomers between $A=198$ and 210. The measured isotope shifts were calibrated with the charge radii of the

stable isotopes extracted from a combined analysis of muonic X-ray shifts and elastic electron scattering³⁶. The specific mass effect disappears within the uncertainty of approximately 10 times the normal mass shift. However, the uncertainty arising from the calibration is the larger part of the total error of the final result.

The scaling uncertainty cannot be reduced when using the nuclear parameters deduced from electronic K_{α} -X-ray shifts³⁴. The quoted isomeric shift between the ground state and the 9^{-} isomer $^{202-202m}\text{Pb}$ $\delta\langle r^2 \rangle = (0.0018 \pm 0.0004)$ fm^2 is not affected by the uncertainty in the mass shift. The overall trend of the variation of the ms charge radii is superimposed by an odd-even staggering as observed in other mass regions. The comparatively large increase of the

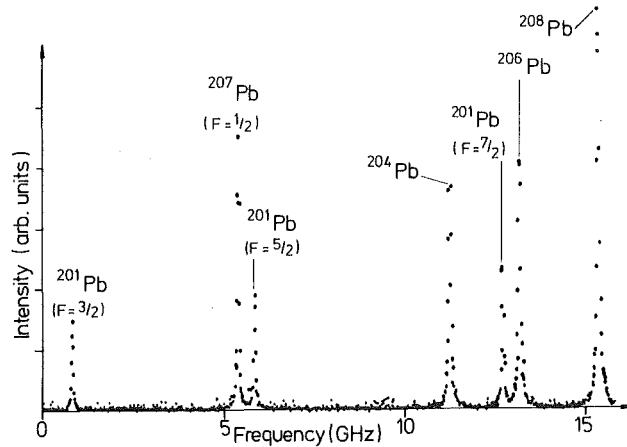


FIGURE 14. Laser induced fluorescence spectrum from a sample containing 2 ng ^{201}Pb ($T_{1/2} = 9.4$ h) and stable lead isotopes for calibration.

radius (^{210}Pb) at the beginning of a neutron shell is also known from many other cases and empirically correlated with corresponding binding energy changes. The droplet model reproduces fairly well the general trend of the radii without

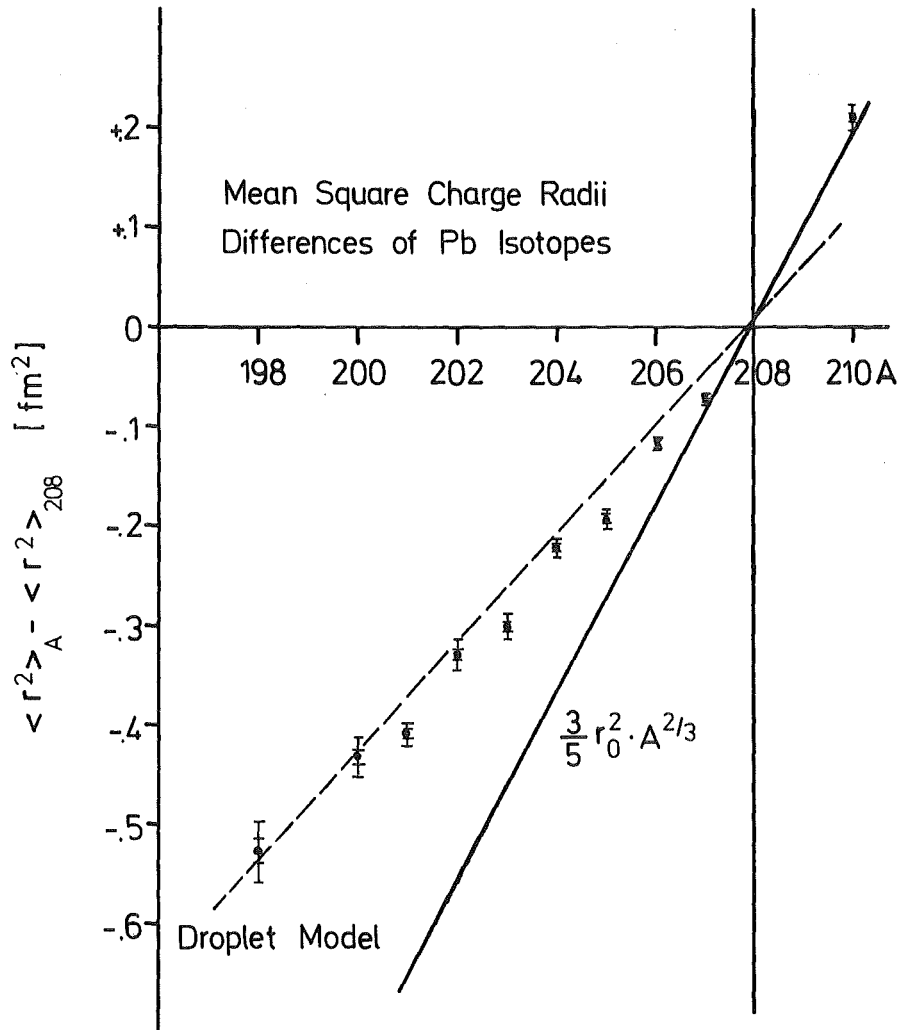


FIGURE 15. Variation of the ms charge radii in Pb isotopes. The error bars include the uncertainties from the calibration by muonic X-ray shifts in stable isotopes.

any additional contribution from a variation of the ms deformation. We note that the quadrupole moments extracted from the measured B-factors of the odd-isotopes (see refs. 6,7) are close to or consistent with zero (with exception of that of ^{202m}Pb). Simultaneously, the droplet model predicts a neutron skin for ^{208}Pb , in agreement with a neutron-proton radius difference $\Delta\langle r^2 \rangle_{np}^{1/2} \cong 0.2$ fm found by high energy proton and alpha-particle scattering^{37,10}.

The experimental data call for more refined theoretical studies and enable serious tests of microscopic calculations performed on the basis of a multi-configuration shell model³⁸. The most challenging feature appears to be the

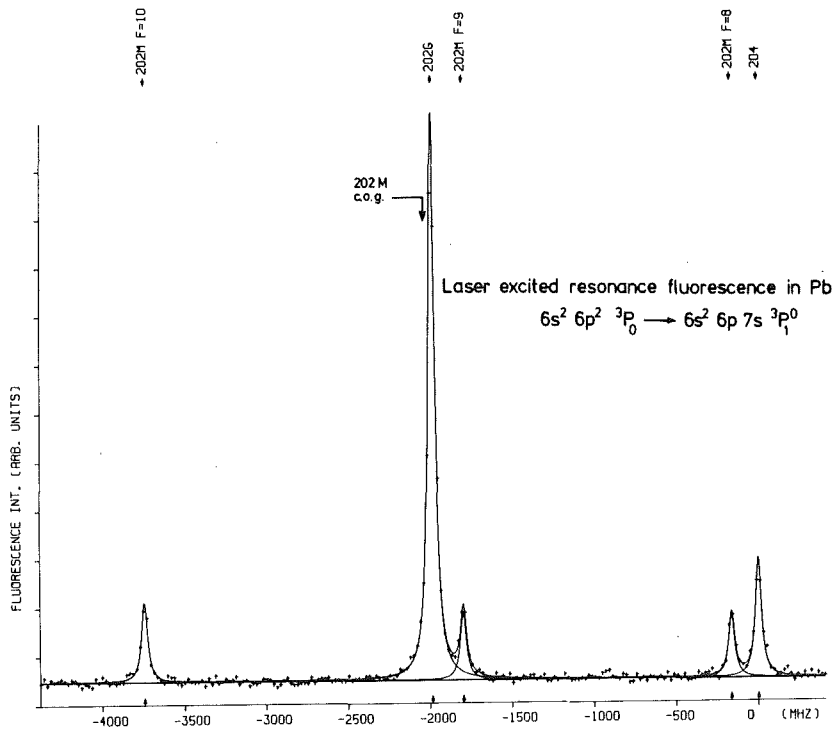


FIGURE 16. Laser spectroscopy of the $^{202m}\text{-}^{202}\text{Pb}$ isomeric shift.

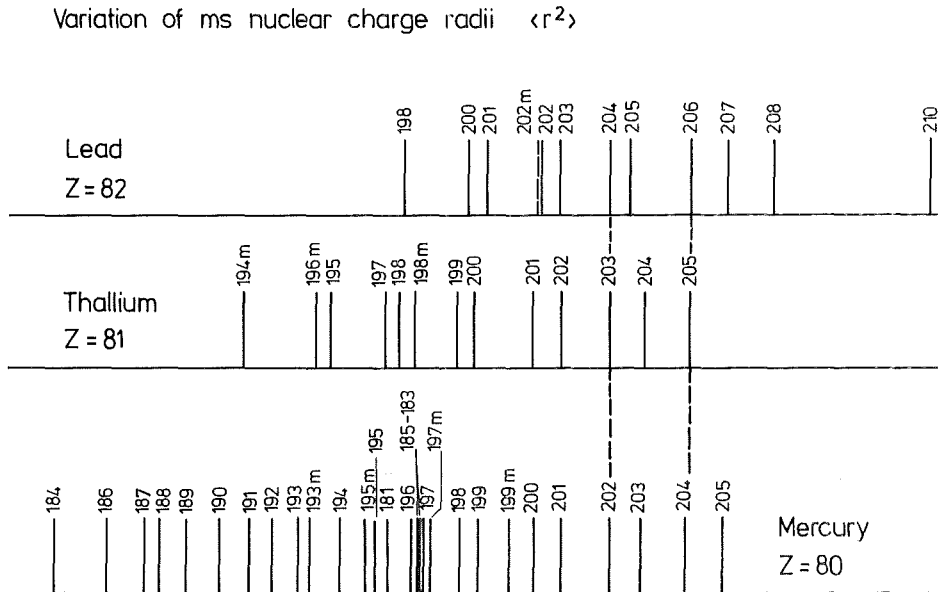


FIGURE 17. Relative isotope shifts in mercury, thallium and lead nuclides ($\langle r^2 \rangle^{N=124} - \langle r^2 \rangle^{N=122} \cong 1$).

long standing problem of odd-even staggering in the radii. The richness of information available (Fig. 17) is steadily increasing since those early days of our century when structures of atomic lines, "finer than fine structure", were discovered by interferometric studies (Fig. 18).

CONCLUDING REMARKS

We considered some representative examples of laser induced atomic beam fluorescence spectroscopy investigating hyper-fine structures and isotope shifts of stable and unstable nuclides in isotopic chains. This particular laserspectroscopic technique enables high precision measurements with

1909.

Nº 10.

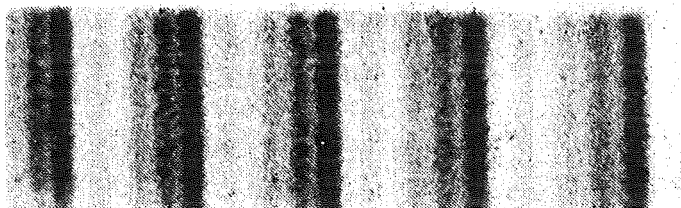
ANNALEN DER PHYSIK.

VIERTE FOLGE. BAND 29.

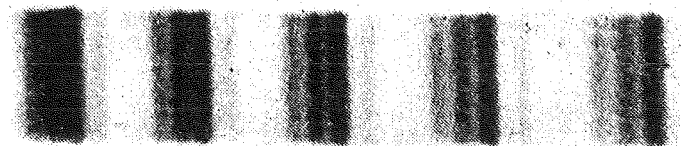
1. *Die Beschaffenheit
der Spektrallinien der Elemente. I;*
von *L. Jantock.*

(Mittellung aus der Physikalisch-Technischen Reichsanstalt.)
(Hierzu Taf. VII.)

5374



4245



3. Blei.

Fig. 18 Early observations of hyperfine structure
in spectral lines of lead samples

very dilute samples, and even applied "off line" it proves to be a rich source of relevant nuclear structure information, in particular when interacting with findings of gamma-ray spectroscopy, the study of X-rays in ordinary and muonic atoms, and electron and hadron scattering.

ACKNOWLEDGEMENTS

The basis of this talk are experimental results obtained by a group which is identical to the authors of refs. 3 to 7. In addition, we would like to thank Mrs. E. Maaß for her labours in preparing the manuscript.

REFERENCES

1. D.A. Jackson and H. Kuhn, Proc. R. Soc. London A148 (1935) 335
2. G.W. Greenlees, D.L. Clark, S.L. Kaufman, D.A. Lewis, J.F. Tonn and J.H. Broadhurst, Opt. Comm. 23 (1977) 236.
3. G.P. Nowicki, K. Bekk, S. Göring, A. Hanser, H. Rebel, and G. Schatz, Phys. Rev. Lett. 39 (1977) 332; Phys. Rev. C18 (1978) 2369.
4. K. Bekk, A. Andl, S. Göring, A. Hanser, G. Nowicki, H. Rebel and G. Schatz, Z. Phys. A291 (1979) 219
H. Rebel, K. Bekk, G. Nowicki, G. Schatz, Nukleonika 25 (1980) 145.
5. A. Andl, K. Bekk, S. Göring, A. Hanser, G. Nowicki, H. Rebel, G. Schatz, and R.C. Thompson, European Conf. on Atomic Physics, Heidelberg, April 6-10, 1981, Abstract 5A, I, 200, and to be published. A. Andl, KfK 3191 (July 1981).
6. R.C. Thompson, A. Hanser, K. Bekk, G. Meisel, and D. Frölich, Z. Phys. A 305 (1982) 89.
7. R.C. Thompson, A. Hanser, M. Anselment, S. Göring, G. Meisel, H. Rebel, G. Schatz, contrib. to this conference.
8. D. Habs, H. Klewe-Nebenius, K. Wisshak, R. Löhken, G. Nowicki and H. Rebel, Z. Phys. 267 (1974) 149.
9. E. Friedman, H.J. Gils, and H. Rebel, Phys. Rev. C25 (1982) 1551.
10. H.J. Gils, H. Rebel, J. Buschmann, H. Klewe-Nebenius, G.P. Nowicki, and W. Nowatzke, Z. Phys. A279 (1976) 55 - Phys. Rev. C13 (1976) 2159.
11. H. Vogg and R. Härtel, Journ. Radioanalyt. Chem. 37 (1977) 857.
12. P.E.G. Baird, R.J. Brambley, K. Burnett, D.N. Stacey, D.M. Warrington, G.K. Woodgate, Proc. Roy. Soc., London A365(1979) 567.
13. G. Schatz, Proc. IV. Int. Conf. Rottach-Egern, June 11-15, 1979, 534.
14. E.C. Seltzer, Phys. Rev. 188 (1969) 1916.
15. O.I. Sumbaev, A.F. Mezentsev, V.I. Marushenk, A.S. Ryl'nikov and G.A. Ivanov, Sov. Journ. Nucl. Phys. 9(1969) 529.
16. W. Fischer, M. Hartmann, H. Hühnermann, and H. Vogg, Z. Phys. 267 (1974) 209.
17. H. Heilig and A. Steudel, Atomic Data and Nuclear Data Tables 14 (1974) 613.

18. H.J. Emrich, G. Fricke, M. Hoehn, K. Käser, M. Mallot, H. Miska, B. Robert-Tissot, D. Rychel, L. Schaller, L. Schellenberg, H. Schneuwly, B. Shera, H.G. Sieberling, R. Steffen, H.D. Wohlfahrt, and Y. Yamazaki, Proc. 4th Int. Conf. on Nuclei Far from Stability, Helsingør, Denmark, June 7-13, 1981, Vol. I, 33.
19. R. Abela, J. Wuest, B. Effenberger, W. Kunold, M. Schneider and L.M. Simons, Contribution to the Nuclear Physics Spring Meeting (DPG), Karlsruhe, March 22-26, 1982, Physikal. Verhandl. 6/1982.
20. W.D. Myers and W.J. Swiatecki, Ann. of Phys. 55 (1969) 395.
W.D. Myers, Droplet Model of Atomic Nuclei IFI-Plenum, New York, 1977.
W.D. Myers, "Droplet Model Predictions of Charge Moments", Talk given at this conference.
21. R. Neugart, F. Buchinger, W. Klempt, A.C. Müller, E.W. Otten, C. Ekström, and J. Heinemeier, Hyperfine Interaction 9, (1981) 151 and to be published.
22. H. Rebel, IOP Conference "Trends in Nuclear Structure Physics", University of Manchester, April 16-18, 1980 (KfK 2974).
23. J. Friedrich, in "What Do We Know about the Radial Shape of Nuclei in the Ca Region?", Proceed. Karlsruhe International Discussion Meeting, May 2-4, 1979 (KfK 2830) eds. H. Rebel, H.J. Gils and G. Schatz.
24. H.D. Wohlfahrt, E. Shera, M. Hoehn, Y. Yamazaki, G. Fricke and R. Steffen, Phys. Lett 73B (1978) 131.
25. E. Bergmann, P. Bopp, Ch. Dorsch, J. Kowalski, F. Träger and G. zu Putlitz, Z. Phys. A244 (1980) 319.
26. H. Überall, Electron Scattering from Complex Nuclei, (Academic Press, New York, 1971).
27. J. Friedrich and N. Voegler, Nucl. Phys. A373 (1982) 192.
28. B.A. Brown, S.E. Massen and P.E. Hodgson, J. Phys. G, Nucl. Phys. 5 (1979) 1635.
29. J. Talmi, private communication (1981).
30. L. Janicki, Ann. Phys. (4) 29 (1909) 833.
31. H. Kopfermann, Z. Phys. 75 (1932) 363.
32. P. Brix, H. von Buttler, F.G. Houtermans, and H. Kopfermann, Z. Phys. 133 (1952) 192.
A. Steudel, Z. Phys. 133 (1952) 438.
33. J. Lindgren, A. Timmermann, and E. Matthias, European Conf. on Atomic Physics, Heidelberg, April 6-10, 1981, Abstracts 5A, I, 235.
34. G.L. Borchert, O.W.B. Schult, J. Speth, P.G. Hansen, B. Jonson, H. Ravn and J.B. McGrory, Proc. 4th Int. Conf. on Nuclei Far from Stability, Helsingør, Denmark, June 7-13, 1981, Vol. I, 56.
35. F. Moscatelli, O. Redi, R.L. Wiggins, and H.H. Stroke, Europ. Conf. on Atomic Physics, Heidelberg, April 6-10, 1981, Abstract 5A, I, 200.

36. G. Fricke, H. Miska and D. Rychel, private communication.
37. G.W. Hoffmann, L. Ray, M. Barlett, J. McGill, G.S. Adams, G.J. Igo, F. Irom, A.T.M. Wang, C.A. Whitten, Jr., R.L. Boudrie, J.F. Amann, C. Glashausser, N.M. Hintz, G.S. Kyle and G.S. Blanpied, Phys. Rev. C21 (1980) 1488.
38. J.B. McGrory, "Shell Model Calculations of Nuclear Charge Radii", Talk at this conference.
39. E.B. Shera, H.D. Wohlfahrt, M.V. Hoehn and Y. Tanaka contr. to this conference - Phys. Lett. 112B(1982)124
40. H.H. Stroke, private communication (1982).
41. F. Moscatelli, private communication (1982).
42. E. Matthias, private communication (1982).
J. Lindgren, E. Matthias and A. Timmerman,
contrib. to this conference.

Appendix A IMPROVED CALIBRATION OF OPTICAL ISOTOPE SHIFTS
IN BaI BY MUONIC X-RAY DATA

During the conference the Los Alamos group ³⁹ presented new experimental data of X-ray measurements in muonic atoms of stable Ba isotopes ¹³⁴⁻¹³⁸Ba. The extracted ms charge radii enable a check of the semi-theoretical values of the electronic factor F_i and of the specific mass shift as used in ref. 4 ($F_i = -3929$. MHz/fm² and $S_i = 0 + N_i$ with the normal mass shift factor $N_i = 31.45$ MHz) and provide an improved calibration of the optical isotope shifts in terms of nuclear radii. The consistency of

Table A1 Mean square charge radius differences extracted from measured optical isotope shifts

- a. Calibration by measured muonic X-ray shifts (Ref. 39)
b. Calibration by semitheoretical values of F_i and S_i (Ref. 4).

A	$\Delta\nu$ MHz	$\delta\langle r^2 \rangle$ ^a fm ²	$\delta\langle r^2 \rangle$ ^b fm ²
137	215.00	-0.071 (7)	-0.059 (4)
136	128.90	-0.041 (6)	-0.041 (8)
135g	260.90	-0.088 (11)	-0.079 (12)
135m	161.70	-0.056 (8)	-0.053 (12)
134	143.00	-0.051 (10)	-0.053 (16)
133g	249.90	-0.087 (14)	-0.084 (20)
133m	202.10	-0.071 (13)	-0.072 (20)
132	167.90	-0.062 (14)	-0.067 (24)
131	249.20	-0.089 (18)	-0.093 (29)
130	207.30	-0.077 (19)	-0.086 (33)
129g	312.30	-0.112 (23)	-0.117 (38)
129m	362.70	-0.128 (24)	-0.130 (38)
128	271.10	-0.100 (24)	-0.111 (42)
126	355.80	-0.130 (30)	-0.142 (51)
124	447.00	-0.163 (36)	-0.175 (60)
139	-473.00	0.154 (15)	
140	-1075.00	0.351 (39)	
141	-1505.30	0.491 (49)	
142	-2019.00	0.659 (65)	
143	-2493.00	0.813 (98)	
144	-3027.00	0.987 (98)	
146	-3893.00	1.270 (125)	

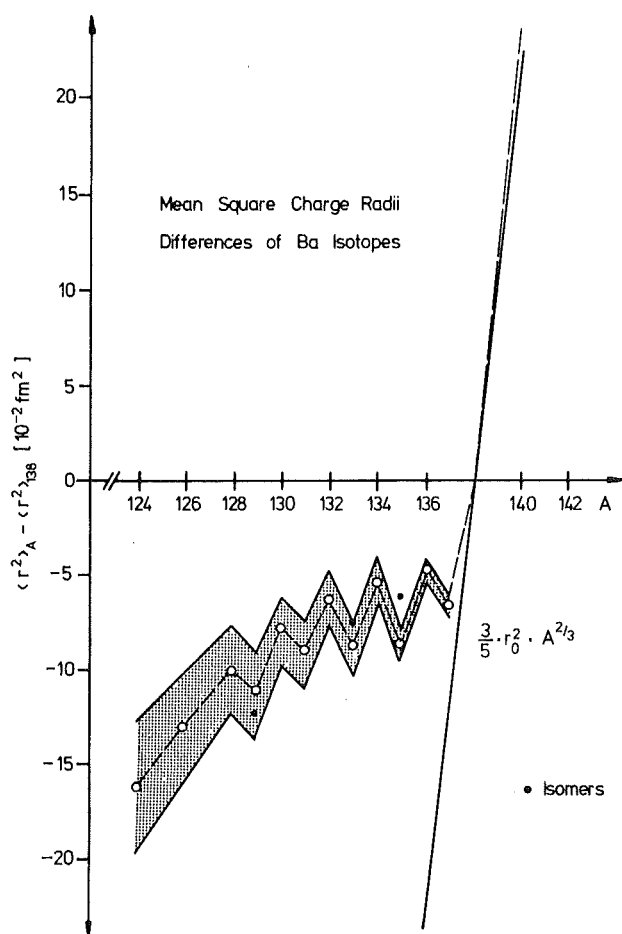


Fig. A1

Differences of ms charge radii of Ba nuclei as extracted from optical isotope shifts and calibrated by muonic X-ray data.

both sets of data is confirmed by a King plot with the results of the stable isotopes, resulting in an electronic factor

$$F_i = -(3085.88 \pm 302.56) \text{ MHz/fm}^2$$

and practically vanishing total mass shift

$$M_i = N_i + S_i = 7 \pm 13 \text{ MHz}$$

implying a specific mass shift contribution of

$$S_i = -24 \pm 13 \text{ MHz.}$$

Table A1 presents the variation of nuclear charge radii based on the experimental results given by ref. 4 ($A < 138$) and ref. 21 ($A > 138$). For convenience the previously given $\delta\langle r^2 \rangle$ values are given by the table. The quoted errors include the errors from calibration (actually the dominating part). As displayed in Fig. A1 the new muonic X-ray data reduce the systematic uncertainties considerably.

Appendix B NUCLEAR CHARGE RADII OF Pb ISOTOPES

For completeness we present the tabulated results of high resolution laser spectroscopy of stable and radioactive lead samples as reported by Thompson et al.⁷. The measured isotope shifts were calibrated with the nuclear parameters of stable lead isotopes obtained by a combined analysis of muonic X-ray shifts and elastic electron scattering³⁶. Using these data the King plot procedure results in a mass shift contribution of $(-7.5 \pm 12.) \times \text{NMS}$, which is consistent with empirical systematics¹⁷ of ns^2 - $nsnp$ transitions. The results of the experiments are summarized in Table 1 and Table 2. The odd-even staggering clearly

TABLE B1 Measured values of isotope shifts relative to ^{208}Pb . Atomic beam absorption spectroscopy results³⁵ are shown for comparison. The quoted uncertainties of $\delta\langle r^2 \rangle$ include uncertainties from the calibration by muonic X-ray shifts. The statistical uncertainties of the experimental results are much smaller.

Isotope	Isotope Shift [MHz]		$\delta\langle r^2 \rangle$ [fm^2]	γ
	This work	Moscattelli 1981		
198	-9848.4(5.)	-	-.5280 (119)	-
200	-8094.1(3.5)	-	-.4324 (77)	-
201	-7727.6(3.)	-	-.4095 (44)	0.38 (10)
202	-6193.7(3.5)	-6134 (100)	-.3300 (48)	-
202m	-6230.4(5.)	-	-.3318 (46)	-
203	-5749. (5.)	-5810 (90)	-.3033 (37)	0.44 (8)
204	-4212. (2.5)	-4257 (90)*	-.2238 (27)	-
205	-3712.6(3.0)	-3750 (120)	-.1946 (38)	0.50 (7)
206	-2226.6(2.5)	-2235 (20)	-.1177 (13)	-
207	-1390.9(2.5)	-1395 (20)	-.0722 (24)	0.75 (3)
208	0	0	0	-
210	+3973.7(3.5)	-	+.2021 (136)	-

*This value⁴⁰ differs from the value quoted by misprint in Ref. 25.

shown by the nuclear radii is presented in Table I by values of the usual staggering parameter

$$\gamma = 2 [\langle r^2 \rangle_{N+1} - \langle r^2 \rangle_N] / [\langle r^2 \rangle_{N+2} - \langle r^2 \rangle_N].$$

TABLE B2 Measured A and B factors, and values of the derived electromagnetic moments. Magnetic moments are scaled to the value of ^{207}Pb (neglecting any hyperfine anomaly correction). The values of the quadrupole moment are derived using results of atomic structure calculations by Moscatelli⁴¹ and are only accurate within a scaling error of $\pm 45\%$.

Isotope	A factor (MHz)	Magnetic moment (n.m.)	B factor (MHz)	Q (eb)
207	8807.2(3.0)	0.5783	-	-
205	2115.7(1.5)	0.6946(7)	-26.(6)	0.14(3)
203	2040.3(2.0)	0.6698(8)	-11(10)	0.06(3)
202m	-187.9(1.0)	-0.2221(12)	-67(15)	0.36(8)
201	2007.5(2.0)	0.6591(8)	+ 1(10)	-0.01(5)

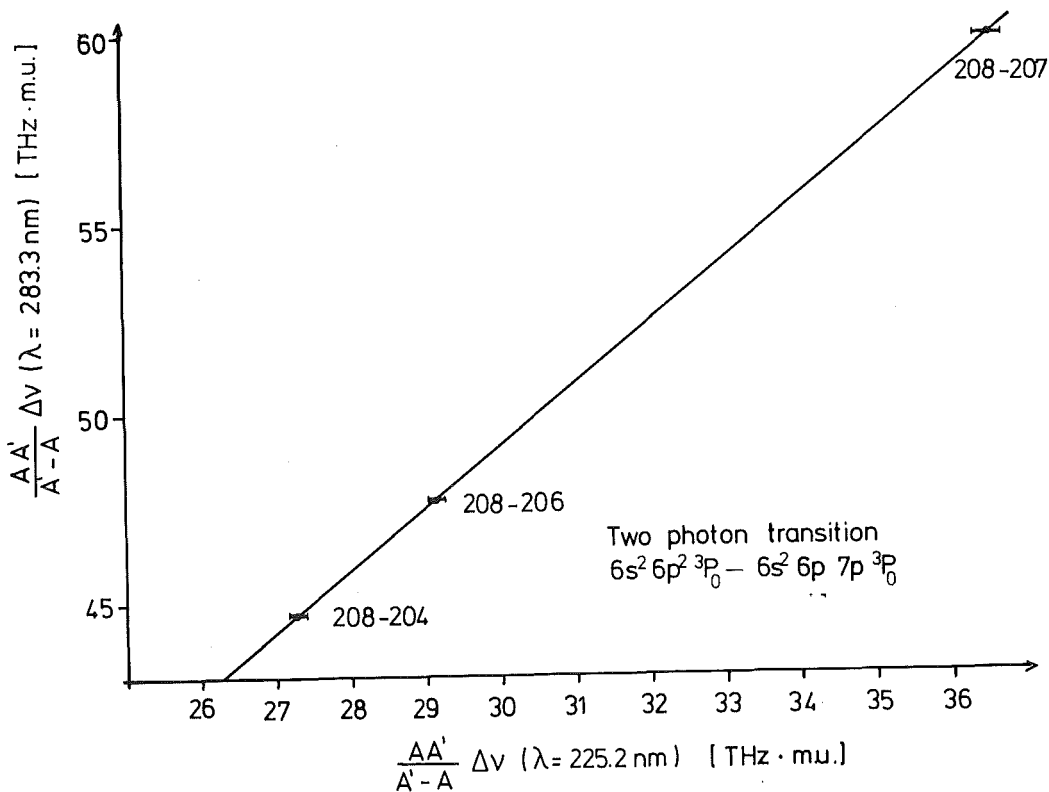


Fig. B1 King plot of the $6s^2 6p^2 \ ^3P_0 \rightarrow 6s^2 6p 7s \ ^3P_1$ resonance transition⁷ against the $6s^2 6p^2 \ ^3P_0 \rightarrow 6s^2 6p 7p \ ^3P_0$ two-photon transition³³ in stable lead isotopes.

Fig. B1 demonstrates the consistency of the results with experimental data obtained by two-photon spectroscopy of the $6p^2\ ^3P_o - 6p\ 7p\ ^3P_o\ (^3D_2)$ transitions in stable lead isotopes^{33,42}. Lindgren et al.⁴² derived values for the electronic factors F_i by atomic structure calculations and calibrated the optical shift by assuming the total mass shift $M_i = 0$. The resulting $\delta\langle r^2 \rangle$ values reported at the conference are in good agreement with the values given in Table B1.